



Supplementary Material for **Earth and Moon impact flux increased at the end of the Paleozoic**

Sara Mazrouei*, Rebecca R. Ghent, William F. Bottke, Alex H. Parker,
Thomas M. Gernon

*Corresponding author. Email: sara.mazrouei.seidani@mail.utoronto.ca

Published 18 January 2019, *Science* **363**, 253 (2017)

DOI: 10.1126/science.aar4058

This PDF file includes:

Materials and Methods
Supplementary Text
Figs. S1 to S6
Tables S1 and S2
References

Other Supplementary Material for this manuscript includes the following:
(available at www.sciencemag.org/content/363/6424/253/suppl/DC1)

Data File S1

Materials and Methods

Statistical Analysis of Lunar and Terrestrial Crater Ages

To evaluate our simple piecewise-constant cratering rate model for the lunar craters, we applied an Approximate Bayesian Computation rejection (ABCr) sampler method, as follows.

Previous work showed that there is an inverse relationship between crater age and Diviner rock abundance (RA), specifically the 95th percentile Diviner rock abundance value (RA_{95/5}), for nine lunar index craters with independently derived ages (2). By taking a regression through those points, it became possible to calculate a crater's formation age from a measurement of RA. For this work, we wanted to update all of the input parameters in (2) with our latest knowledge of the data:

1. We used an updated age of 164 ± 1.4 Myr for index crater Aristarchus based on new ejecta blanket counts that sought to eliminate the effects of self-secondary cratering (26).
2. All index craters with ages determined from superposed crater spatial density values were assigned self-consistent age uncertainties (see below).
3. The previous study (2) used RA retrievals performed using Diviner data collected between July 5, 2009 and November 30, 2010, which covered the region between 60°S and 60°N (1). Our updated RA dataset for 80°S and 80°N was derived using observations to September 2, 2012 (1, 23, 30).
4. As for the original analysis, we further refined the RA values of all analyzed lunar craters by excluding terrains interior to crater rims, where mass wasting can replenish the block population, large melt deposits, where small superimposed craters produce many fresh rocks, and regions with steep local slopes, where rocks can be easily covered with fine-grained material.

We modeled the age-RA₉₅ relationship based on these index craters using:

$$RA_{95/5} = a (\text{age} / \text{Myr})^b \quad (\text{S1})$$

We sought to determine the posterior PDF for the parameters a and b given the index craters' measured RA₉₅ values and their ages derived from superposed craters. However, published uncertainties for the ages of these index craters reflect counting statistics of superposed craters, but do not reflect other potential sources of uncertainty (such as increasing difficulty in assessing underlying terrain type, unacknowledged uncertainty in the production function, and other processes).

To account for the potential for additional unacknowledged sources of uncertainty in the index crater ages, we adopted the following log-likelihood function for the parameters in equation S1 and an additional previously-unaccounted for uncertainty term (added in quadrature with the published uncertainties) that scales linearly with age (with proportionality constant c ; that is, $\sigma_{tot}^2 = \sigma_{age}^2 + c^2 age^2$, where σ_{tot} implied total age uncertainty, σ_{age} is the published crater age uncertainty, age is the published crater age, and c is the age uncertainty scaling factor):

$$\ln L(\text{age} | RA_{95}, a, b, c) = \frac{-1}{2} \sum_{i=0}^n \left(\frac{(\text{age}_i - (RA_{95,i}/a)^{1/b})^2}{\sigma_{age,i}^2 + c^2 \text{age}_i^2} + \ln(\sigma_{age,i}^2 + c^2 \text{age}_i^2) \right) \quad (\text{S2})$$

with i the subscript of a given index crater and n the total number of index craters. When published uncertainties were asymmetric, their average was adopted for age.

Adopting this log-likelihood as well as non-informative priors for model parameters (uniform in $\ln(a)$, b uniform over real values, uniform in $\ln(c)$) we used *emcee* (31) to generate a sample of 10^5 model parameters drawn from the posterior probability distribution defined by the data and the model. The resulting 95% credible intervals on the parameters are: $0.23 < a < 0.73$, $-0.65 < b < -0.43$. The parameters at the peak of the posterior PDF are $a = 0.33$ and $b = -0.50$. The posterior PDF of the constant of proportionality (c age) for the additional uncertainty term in Eq. S2 is found to peak at $c \sim 0.30$, with a 95% credible interval 0.20 - 0.81.

We applied the Approximate Bayesian Computation (ABC) method (31-34) to assess both the posterior PDF of the parameters of a piecewise cratering rate model, and the Bayesian evidence in favor of the piecewise-uniform model over a simple uniform model. The ABCr framework we utilized was derived from (34), modified to use non-parametric similarity tests in the place of summary statistics to enable accurate assessment of Bayes factors.

We performed 2×10^7 ABCr trials, in each of which we randomly selected the following parameters: (i) an RA-age regression from the posterior PDF generated above; (ii) either a uniform model or piecewise uniform model, with equal prior probability; and (iii) parameters for this model. For the piecewise uniform model, the break age was selected from a uniform prior over the domain of ages defined by the calibration craters, and the rate ratio R for times before the break, defined as early, and after the break, defined as late, was $R = R_{\text{late}} / R_{\text{early}} = f/(1-f)$. Here f is drawn from an arcsine distribution prior (the Jeffreys' prior (35) for a Bernoulli trial success rate parameter). We then generated a synthetic dataset (of equal sample size to our observed dataset) by sampling from the selected model given each set of these parameters, and conducted a two-sample Anderson-Darling (AD) test (36) on the synthetic and observed datasets.

We identified the trials (and the parameters proposed in them) that resulted in the lowest Anderson-Darling s-statistics (selecting the 0.01% best cases), indicating the minimum discrepancy between the synthetic and observed datasets (given sampling stochasticity). We take the distributions of parameters from those accepted trials to approximate the posterior PDF of the model parameters, and the ratio of the rates at which piecewise-uniform trials were selected by this metric over uniform trials as approximating the Bayes factor for these two models; the latter is a measure of the evidence in favor of the piecewise-uniform model over the uniform model.

To confirm robustness, we also conducted identical analyses with an additional distance metric, adopting the Kolmogorov–Smirnov (KS) test D-statistic instead of the AD-test s-statistic. Like the summary-statistic free ABC technique (37), both of these metrics share the property that the entire sequence of observations are used in the distance metric, making them valid for computing Bayes factors in an ABC framework (38). Both metrics produced Bayes factors and posterior probability distributions that were identical within their sampling uncertainties.

To evaluate the effect of including the terrestrial crater population in addition to the lunar population, we repeated this process while simultaneously modeling the lunar and terrestrial crater samples (where the terrestrial sample was modeled over an interval limited to 0-650 Myr). Most terrestrial crater ages are derived from radiometric analyses,

and are thus not subject to the correlated absolute age uncertainties of the lunar craters due to the uncertainty in our age- RA_{95} model parameters. Our results are shown in Figure S1. For the lunar crater sample alone, and marginalizing over all possible RA-age regressions and age-uncertainty scaling factors, we find a Bayes factor of ~ 11 in favor of the piecewise model relative to a uniform model, indicating evidence for the piecewise model (39). The 95% credible interval for the break age of the piecewise model is 220-770 Myr; the posterior PDF peak is at 400 Myr. The 95% credible interval for the rate increase factor in recent times is 1.4 – 20.6, and the posterior PDF peaks at 2.1. The terrestrial craters with $D \geq 20$ km and age ≤ 650 Myr are generally consistent with the modal lunar cratering piecewise uniform distribution (KS-test p-value ~ 0.14), and are strongly inconsistent with a uniform distribution (KS-test p-value ~ 0.002). The inclusion of the terrestrial craters raises the Bayes factor in favor of the piecewise model to 160, and shrinks the 95% credible interval for break age to 150-550 Myr (posterior PDF peak at 290 Myr), and the 95% credible interval for the rate increase factor to 1.7-4.7 (posterior PDF peak at 2.6). The posterior PDF of the age- RA_{95} regression parameters (a , b) was found to peak at values similar to those from the lunar analysis alone, at $a \sim 0.24$ and $b \sim -0.51$.

As an additional robustness test, we considered an alternate scheme for defining the sample of index-craters that are used to estimate the parameters of the age- RA_{95} model in S1. In this test, we used only Copernicus and Tycho as index craters, two large craters with absolute age estimates derived from returned lunar samples. This provides an alternative analysis that requires no assumptions about the uniformity of the production rate of small lunar craters. Using the age- RA_{95} parameters derived from these two craters' alternate absolute ages, the Bayes factor for the lunar-only analysis remains as high as ~ 7 and the median break age shifted to ~ 630 Myr. Despite the vastly reduced sample size, this analysis provides a consistency check and supports our finding that the large body impact flux experienced a substantial change over the last 1 Gyr.

The Small and Large Body Impact Flux on the Moon

It is often asserted that the impact flux on the Moon has been constant for the last 3 Gyr (e.g., 40). This is inconsistent with our result that the Earth and Moon experienced an increase in the production rate of diameter $D \geq 10$ km craters at approximately 290 Myr. For this reason, we examine the origin of this assertion, where it can be reasonably applied, and whether it has any limitations.

The primary evidence that the Earth and Moon experienced a constant impact flux over the last 3 Gyr comes from three lunar terrains whose absolute ages and crater spatial density values are known. From oldest to youngest, these locations are (i) the Apollo 12 landing site, with an age of ~ 3.2 Ga; (ii) Copernicus crater, whose ~ 0.8 Ga age comes from Apollo 12 samples believed to be derived from an ejecta ray of Copernicus crater; and (iii) Tycho crater, whose ~ 0.1 Ga age is based on exposure ages of Apollo 17 samples taken from a landslide plausibly triggered by Tycho ejecta (e.g., 41-43). All of these terrains are relatively small, so the largest craters superposed on them are usually $D < 1$ km. The smallest craters counted on them are $D >$ few meters. Assuming projectiles striking the Moon make craters with 20 times higher diameter than the impacting body, the superposed craters on these terrains were created by projectiles that were approximately sub-meter to several tens of meters in diameter.

An interpolation between the three above points in (surface age, crater spatial density) space yields a small-crater production rate and a small-asteroid impact rate that is approximately constant over the last 3 Gyr (e.g., 40, 57). The inferred impact rate from these values is also broadly consistent with the population of sub-meter and meter-sized impactors found to strike the Earth today (e.g., 44). Accordingly, small craters superposed on planetary features over the last 3 Gyr are often used as a steady clock to date the absolute ages of events of geologic features on the Moon and other terrestrial planets (e.g., 9, 57).

We apply the idea of a constant small body impact flux in two ways. First, we assume that any large lunar craters that formed over the last billion years can be dated to reasonable accuracy using superposed small craters (e.g., King crater, labeled as “K” in Fig. 1). We expect that age errors for these large craters should be relatively small because most of the surface age and crater spatial density constraints discussed above are from the < 1 Gyr time period. Effectively, this places limitations on how much the small body impact flux can plausibly change over the last Gyr.

Second, we assume that a constant influx of small impactors, combined with the thermal effects of lunar cycling, produces a steady breakdown rate of lunar rocks and boulders. Rock destruction serves as a more straightforward clock than small-superposed craters because rock abundances on a terrain can be quantified remotely using Diviner thermal data. While the details of the mechanisms pulverizing rocks and boulders on the Moon are unknown, it is enough for our purposes to know these rock breakdown rates are likely to be constant. The evidence above suggests that the small body impact flux has been fairly constant over the last Gyr; there are no indications to believe that the solar flux has varied substantially over same time period. Figure 1 shows that rock abundances undergo comminution in a manner that can be defined by a simple function.

We also consider the lunar impact flux in terms of production. Most bodies that hit the Earth and Moon come from the main asteroid belt (e.g., 45). They are driven out of the main belt and onto planet-crossing orbits by the Yarkovsky and YORP (Yarkovsky-O’Keefe-Radzievskii-Paddack) effects, thermal radiation forces and torques that cause small objects to undergo semi-major axis drift and spin vector modifications, respectively, as a function of their spin, orbit, and material properties (46). The timescale for most bodies smaller than a few tens of meters to escape the main belt is longer than their collisional lifetime. This implies that the majority of small bodies reaching planet-crossing orbits do so via a collisional cascade, with the small body population continually replenished by disruption events among larger bodies (47, 48). This effectively places the small body population into a steady state.

Collisional and dynamical models indicate that new size-frequency distributions introduced into the main belt as a byproduct of a cratering or disruption event gradually take on the shape of the background main belt size-frequency distribution, with meter-sized objects ground down within a few Myr to tens of Myr (47, 48). This rapid breakdown rate means that it is difficult for newly created fragment distributions to dominate the background main belt population at small sizes for very long. Accordingly, substantial changes to the net small body flux escaping the main belt are unlikely to last more than a few Myr to a few tens of Myr, even if the breakup occurs next to a resonance that can take the material immediately to planet-crossing orbits. The fast collisional

evolution of small bodies in fragment distributions may help explain why the small body impact flux on the Moon has remained approximately constant for 3 Gyr.

The net escape rate of large asteroids from the main belt, however, is different. We define “large bodies” as those capable of making $D \geq 10$ km craters on the Earth and Moon (i.e., probably $D > 0.5$ km asteroids). The surface age and crater spatial density constraints are not applicable in this size range, except in how small superposed craters can be used to date large craters. Accordingly, we do not know whether the large body impact flux on the Earth and Moon has been constant for the last 3 Gyr.

The available constraints for the large body impact flux hitting the Earth and Moon over the last 1 Gyr are contained in the crater size-frequency data and kimberlite distribution in this paper. They support a substantial increase in the large body impact flux at ~ 290 Myr. These results lead us to infer that the small and large body impact fluxes are modestly decoupled.

This assertion is supported by collisional and dynamical evolution models of asteroid breakup events in the main belt. Most large asteroids that strike the Earth and Moon come from the inner main belt via a combination of Yarkovsky/YORP thermal forces and dynamical resonances (45, 46, 49). If a very large asteroid breaks up in this zone, it may be capable of creating enough large fragments to dominate the background population near a main belt escape route for many hundreds of Myr. In turn, these large asteroids will dominate the Earth and Moon impact flux for a comparable time period until collisional and dynamical processes deplete the source population.

Modeling indicates surges of large impactors may be linked to the formation and evolution of large and/or well placed asteroid families; examples include the Baptistina asteroid family (21), the Flora asteroid family (22), the Eulalia and New Polana families (48), and the Gefion family (50). Baptistina is likely < 300 Myr old (21, 51), making it a plausible source for at least a portion of the impact flux increase we found.

We consider in schematic form the effect of varying our assumptions about the small and large crater production rate on the Moon (shown schematically in Fig. S2). Scenario A assumes that small and large crater production rates are decoupled, with the former constant and latter increasing at ~ 290 Myr (Fig. S2a). This is our fiducial interpretation. As discussed above, this is supported by: (i) evidence from the Moon and the current impact flux on Earth that the small body impact flux has been constant over the last 3 Gyr; (ii) large terrestrial craters whose ages were determined by samples show evidence for an increase in the impact flux starting ~ 290 Myr (we assume erosion did not erase large craters formed on stable cratonic terrains), (iii) the ages of large lunar craters derived using Diviner data; (iv) insights from collisional and dynamical evolution modeling work.

In Scenario B the small body and large crater production rates are coupled and constant (Fig. S2b). We assume that the breakdown of lunar boulders, which act as our clock, are destroyed faster than before. This effect would make large craters seem even younger than they do in Fig. S2a. (for the moment, we ignore that this scenario does not match our crater age regression in Fig. 1). The resultant age distribution of large craters, however, would not match terrestrial craters, whose absolute ages are determined from samples. It is also unclear how the main belt would produce these impact fluxes.

Scenario C assumes that the small and large crater production rates are decoupled, with the former decreasing ~ 290 Ma and latter constant (Fig. S2c). This scenario is the

converse of Scenario A. While it does provide an alternative way to explain our results, it is inconsistent with constraints e.g., the small body impact flux is no longer constant over the last 3 Gyr; the age distribution of terrestrial and lunar craters would no longer match; we do not know how it could be produced given our understanding of the collisional and dynamical evolution of the main belt.

We therefore conclude that Scenario A is most consistent with the data and adopt it in our analysis.

Computing the Impact Flux on the Earth using the Lunar Crater Record.

We use the lunar crater record to estimate the impact flux on the Earth over time via the following steps.

Impact Ratio Between the Earth and Moon.

To determine the relative accretion rate between the Earth and Moon, we first need to estimate the typical impact velocities of bodies striking the Earth, with most impactors derived from the main asteroid belt (45, 50, 52).

We used previously published numerical integrations for this purpose (48). Tens of thousands of synthetic main belt asteroids were placed near or in three intermediate source regions for Near Earth Objects (NEOs), with the dynamical definitions of the regions used below described in (48): (i) the ν_6 secular resonance, (ii) the intermediate source Mars-crossers, and (iii) the 3:1 mean motion resonance with Jupiter (45, 48). Model results (45) indicate that very few sizeable terrestrial impactors come from the outer main asteroid belt or comets. Bodies were tracked if they escaped the asteroid belt via Yarkovsky thermal forces and resonances until they struck a terrestrial planet, struck the Sun, or were ejected from the inner solar system via a close encounter with Jupiter (48). Overall, 378, 251, and 48 of the test asteroids hit the Earth, representing 2.96%, 1.79%, and 0.59% of the total escaping populations from each source, respectively (48). The median impact velocities of the test bodies for those sources were 17.8, 19.8, and 21.1 km/s, respectively, while the median velocities at infinity were 13.8, 16.3, and 17.8 km/s, respectively.

To combine these velocities from the three sources, we multiplied the fraction of each population that hit the Earth by their expected contribution to the NEO population (45); 37%, 27%, and 20% of the NEO population comes from sources (i), (ii), and (iii) listed above, respectively. Normalizing these multiplied values such that their sum is 100%, we estimate that 65%, 28%, and 7% of Earth's impactors come from sources (i), (ii), and (iii), respectively. Put together, we find a median impact velocity and velocity at infinity value of Earth impactors to be 18.1 and 14.2 kms^{-1} , respectively. By converting these values to their equivalents for the Moon (53), we obtain an impact ratio between the Earth and Moon of 20.9, or 1.6 per square kilometer.

Observations of 119 meter-sized or larger bolides striking the Earth's atmosphere over the last several decades by space surveillance satellites yield mean and median impact velocities of 17.3 and 16.3 kms^{-1} , and velocities at infinity of 13.1 and 11.8 kms^{-1} , respectively (e.g., 52). These velocity values are slightly lower than those above, producing Earth/ Moon impact ratios of 22-24 and Earth/Moon impact ratios per square kilometer of 1.7-1.8. We cannot determine whether these values are superior to those computed above. Supporting the higher ratios, meter-sized bodies have somewhat

similar orbital distributions to those of larger NEOs (52). However, meter-sized bodies may be more susceptible to disruption near the Sun than kilometer-sized impactors and therefore may have fewer highly eccentric bodies (49). Regardless, these results suggest that a reasonable range of Earth/Moon impact ratios is 21-24, while those per square kilometer is 1.6-1.8.

Calculations of the Terrestrial Impact Flux.

We find that 18 ± 4 lunar craters identified as rocky have $D \geq 20$ km and ages less than 650 Myr (Table S1). Using our calculation that the Earth is impacted 20.9 times more often than the Moon, an Earth/Moon ratio of 1.6 impacts per square kilometer, and that crater scaling relationships between the Earth and Moon are similar, this suggests there should be 376 ± 84 craters of $D \geq 20$ km formed on Earth over 650 Myr. Only 38 ± 6 are known (Table S2), so the ratio yields $(38 \pm 6) / (376 \pm 84)$ or $10.1 \pm 3.2\%$ of the Earth's surface.

Given that most heavily cratered regions on Earth are located on regions that have not experienced substantial erosion over the last 650 Myr, we argue that the value of $10.1 \pm 3.2\%$ of the Earth's surface represents an approximate "crater counting surface". We define this phrase as those terrestrial terrains that have been stable to large crater formation over 650 Myr and accessible enough to humans to have been well searched. If a substantial number of craters were missing from this crater counting surface, or if erosion/burial/exhumation were common, the age/size distribution of large terrestrial craters should be substantially different than observed large lunar craters.

In terms of the expected impact flux, the Moon has $13 (\pm 3)$ $D \geq 20$ km craters that formed < 291 Myr (i.e., the derived age of Ohm crater; its age is close to our preferred breakpoint in Fig. 3), leading to an average production rate of $1.1 (\pm 0.3) \times 10^{-15} \text{ km}^{-2} \text{ yr}^{-1}$. Scaled to Earth, this value becomes $1.7 (\pm 0.5) \times 10^{-15} \text{ km}^{-2} \text{ yr}^{-1}$, whereas estimates from examined terrestrial craters on cratons in North America, Europe, and Australia over the last $\sim 125 \pm 20$ Myr suggest a value closer to $\sim 3 \times 10^{-15} \text{ km}^{-2} \text{ yr}^{-1}$ (54). An alternative interpretation of these curves is that the impact flux has been steadily increasing over the last ~ 290 Myr, with the highest values reached within the last 100 Myr. Taking the $5 (\pm 2)$ identified lunar craters formed over the past 85 Myr (Table S1) and scaling their production to Earth yields $2.5 (\pm 0.8) \times 10^{-15} \text{ km}^{-2} \text{ yr}^{-1}$. Similarly, using the $13 (\pm 4)$ terrestrial craters over the same age (Table S1), combined with a crater counting surface of $10.1 \pm 3.2\%$, yields $3.0 (\pm 1.2) \times 10^{-15} \text{ km}^{-2} \text{ yr}^{-1}$. Both values are consistent with previous estimates (9, 54).

Numerical Methods to Derive an Approximate Terrestrial Crater Counting Surface.

To explore the implications of our estimated crater counting surface of $10.1 \pm 3.2\%$ of the Earth's surface, we examined the terrestrial crater record using numerical simulations.

The standard method to calculate an average crater production rate for a given body is to identify a large stable cratered region of known (or assumed) absolute age, count craters on that terrain, and divide the number of craters of a chosen diameter or larger by the terrain's age. It is unclear, however, how closely we can follow this procedure for terrestrial craters. There are large terrestrial regions where no craters have been found due to a large number of complicating factors, including: young surfaces,

erosive processes efficient at erasing craters in specific regions, ice or water cover, and physical inaccessibility. Examples include the ocean floors, mountain ranges, deserts, ice-covered regions like Antarctica, and high vegetation regions like the Amazon basin. The regions that do have known craters rarely have established counting areas, in large part because it is difficult to quantify how effective crater erasure mechanisms are on different terrains.

To mitigate this uncertainty, previous work (54) estimated a terrestrial crater production rate over the last $\sim 125 \pm 20$ Myr by identifying craters on stable cratons in North America, Europe, and Australia. The precision of the impact flux estimates was limited by the small numbers of craters known on those terrains (54). Alternative methods to discern the terrestrial impact flux are discussed elsewhere (55, 56).

We used a numerical method to estimate the net crater counting area for large terrestrial craters. It requires simplifying assumptions, and therefore is approximate. Our first assumption is that all regions with small and large craters have been well searched for a considerable distance in every direction from that crater. This assertion is hard to prove, but is supported by the fact that the highest crater spatial densities are generally located on stable, physically accessible regions (e.g., North America, Europe and eastern Asia, Australia). Our second assumption is that most 5-15 km diameter craters are located in the same stable regions where larger craters are found and therefore adequately sample stable terrestrial surfaces (Fig. 4). Support for this assertion comes from the age distribution of 5-15 km craters; using ages in the Planetary and Space Science Centre (PASSC) Earth Impact Database (24), we find the resultant distribution is only modestly different from those of $D > 20$ km craters (54).

To compute our model crater counting area, we chose a threshold search distance d_{search} and calculated the area around each terrestrial crater with diameter D . Regions where d_{search} overlapped between craters were only counted once. To determine the net counting area, we used a simple Monte Carlo method. We selected $N = 30,000$ random points on the surface of the Earth and calculated the number N_{search} that were within d_{search} of one of our craters. The net crater counting area, as a function of the Earth's surface area, was N_{search} / N .

In Fig. S4a-d, we show representative examples from our runs. Our goal was to find the d_{search} values that produced modest overlap between most known craters. If the d_{search} values were too small, isolated patches of searched area were produced around each crater; if the d_{search} values were too large, areas with no craters, such as mountain ranges and oceans, began to be covered. This method is subjective and iterative; however, we determined that reasonable values result from $d_{\text{search}} = 500, 550, 600,$ and 650 km. They yield crater counting areas of 9.6%, 10.5%, 12.0%, and 13.3% of Earth's surface, respectively.

These computed values are within the uncertainty of our derived crater counting surface of $10.1 \pm 3.2\%$ of the Earth's surface. Accordingly, these results provide further support that most large craters ($D \geq 20$ km) have withstood erosion over the last 650 Myr.

Supplemental Text

Interpretation of Rayed Craters on the Moon

The presence of crater rays, streaks of fine ejecta radially thrown away from an impact crater during its formation, is often cited as an indication of Copernican ages for lunar craters (9, 57, 58). The Copernican era was originally defined to include all lunar craters younger than 1.1 Gyr (57). Rock obliteration and regolith gardening mechanisms cause many rays to fade into the background as small optically bright ejecta fragments are darkened, broken down and/or mixed in with the surrounding regolith. Because it uses the degradation state of fresh material produced by impacts, dating craters by ray obliteration is potentially analogous to our method. Observations of farside rayed lunar craters have been used to argue that the impact flux increased by a factor of two during the past ~300 Myr (9).

Many rays, however, are compositionally different from the surrounding regolith (10, 58, 59), and this allows them to persist longer than the rocks detected by Diviner or the Copernican boundary age of 1.1 Gyr (10, 57, 58). For example, we only find 11 farside rocky craters with $D \geq 20$ km compared to 28 to 32 farside rayed craters (9, 10). Optical maturity measures, defined by changes in the spectral reflectance of lunar soils over time, suggest that only 13-19 farside rayed craters are younger than Copernicus (9), values within 20-70% of our estimates. The source of the remaining discrepancy is unknown, but optically immature rays sometimes lack rays that can be seen in radar from Earth-based observations, which indicate an absence of the centimeter-sized rocks (60,

61) that give rise to characteristic radar-bright returns. Taken together, these factors imply that rayed craters are challenging to use as a predictor of impact flux changes (9).

The population of rocky craters could be considered an alternative quantitative definition for Copernican-era craters (57). Our age cutoff of ~1 Ga (Fig. 1) is close to the originally proposed interval of 1.1 Gyr for the Copernican era, but our method employs fewer assumptions (e.g., no knowledge is needed of the lifetime of bright crater rays).

Cratonic Erosion and the Kimberlite Record

To produce independent constraints on cratonic erosion through time, we examined the kimberlite record using an extended and updated version of an existing database (25). The published version comprises 4287 entries, of which we selected only well-dated occurrences and appended recently published radiometric dates ($n = 624$; Fig. S5; Data File S1). Data were compiled on the mode of each occurrence (i.e., crater, pipe, root zone or intrusive) and pipe dimensions. Preserved kimberlite craters such as Orapa, Mwadui and Fort à la Corne indicate a low degree of erosion, probably not exceeding 200 m (16). These are typically underlain by pipes, or diatremes (Fig. 4) that extend to 1–1.5 km beneath the surface, which in turn are underlain by root zones typically 1.5–2 km deep (14-16, 62). Intrusives, although mainly restricted to the deep parts of kimberlite pipes (14, 15, 62), are less reliable indicators of erosion depth as they are increasingly recognized at high levels in kimberlite pipes and clusters. However, where isolated (i.e., not part of a cluster of pipes), kimberlite intrusives may signify deep erosion of a kimberlite field. This can be illustrated by examining kimberlites >650 Myr old: the majority of these correspond to isolated occurrences of intrusive or hypabyssal rocks (Fig. S5), presumably the heavily eroded remnants of kimberlite fields. Few complete

pipes are >650 Myr old, and there is evidence that a cluster of these (e.g., in the Kimberley Region, Western Australia), were buried soon after emplacement in intracratonic sedimentary basins.

Whilst thermochronologic constraints and the kimberlite record indicate generally low cratonic erosion (or deposition) rates since ~650 Myr, there are exceptions—particularly along craton margins (e.g. the Appalachian orogen) where tectonic deformation will invariably have led to crater erasure. Another example is the southern African Plateau, where major uplift and erosion of >1–1.5 km of strata during the Late Cretaceous (63, 64) exposed the deep root zones of kimberlite pipes in South Africa and Lesotho. This may have implications for impact crater survival locally, but we argue that the inferred magnitude of erosion is still unlikely to obliterate $D \geq 20$ km craters. For instance, the ~145 Myr Morokweng impact crater (70 km diameter) in South Africa (24) was not erased by this major uplift episode. Similarly, one of the oldest impact craters in Table S2, the ~600 Myr Beaverhead crater in Montana and Idaho (24), is in an area that experienced considerable uplift, most recently during the Laramide orogeny (~80–35 Myr). This event heavily eroded the Beaverhead crater and some North American kimberlites, exposing their root zones (Figs. 4 and S5). These examples demonstrate how preservation levels of well-dated kimberlites can be used as a proxy for the degree of erosion of nearby impact craters.

We consider whether impact craters and kimberlites share the same burial and exhumation history. Burial requires sedimentation, and given the inferred slow sedimentation rates on the cratons (12), many younger kimberlite pipes should have been emplaced into this sedimentary cover (Fig. S6). However, the eventual exhumation of such sedimentary cover—required to expose the older kimberlites and impact craters—would then extensively unroof the deepest parts of younger kimberlite pipes (Fig. S6A), which is not evident in the record (Fig. S5). The dominance of younger volcanic craters and pipes (<400 Myr) is consistent with low sedimentation rates in most cratonic areas (Fig. 4, Fig. S5) (12), ruling out widespread burial of impact craters (Fig. S6). The shared presence of kimberlite pipes and impact craters on stable cratonic surfaces (Fig. 4) provides additional support for limited erosion in these regions (12) over the last 650 Myr—constraining the records of large ($D > 20$ km) terrestrial and lunar impact craters.

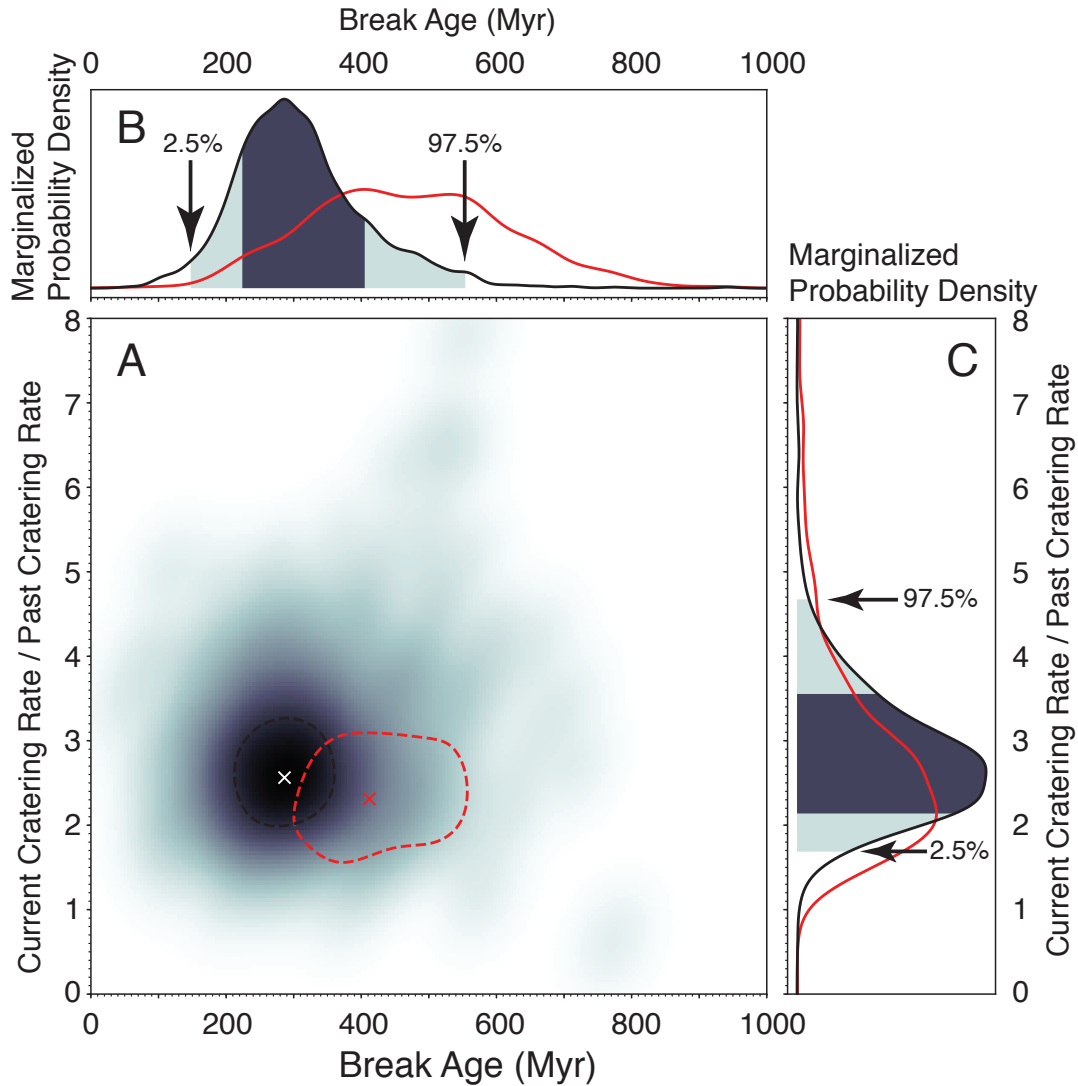


Fig. S1. Increased impact flux by a factor of 2.6. Joint statistical analysis of the ages of the 111 rocky Lunar craters shown in Fig. 1 and the sample of 38 terrestrial craters indicates an increase in impact flux at 290 Myr. **(A)** Two-dimensional representation of the posterior PDF for the ratio of current to past cratering rates (y-axis) versus model break age (x-axis) derived from 2×10^7 trials using the ABCr sampler and a Kernel Density Estimator, derived from the joint terrestrial and lunar crater sample (density plot) and the lunar sample alone (red contour). Dashed contours mark 1-sigma credible region (joint sample: black contour, lunar sample: red contour). Peak PDF density marked by crosses. **(B, C)** Marginalized posterior PDFs for model break ages and cratering rate ratio, respectively, for lunar (red PDF) and lunar + terrestrial (shaded PDF) craters; marginalized 1- σ and 2- σ intervals for parameters derived from joint lunar + terrestrial dataset are marked by dark and light filled portions of the PDFs, respectively. The addition of the terrestrial craters disfavors early break ages and low rate increases, supporting a relatively recent, large increase in the cratering rate across both bodies.

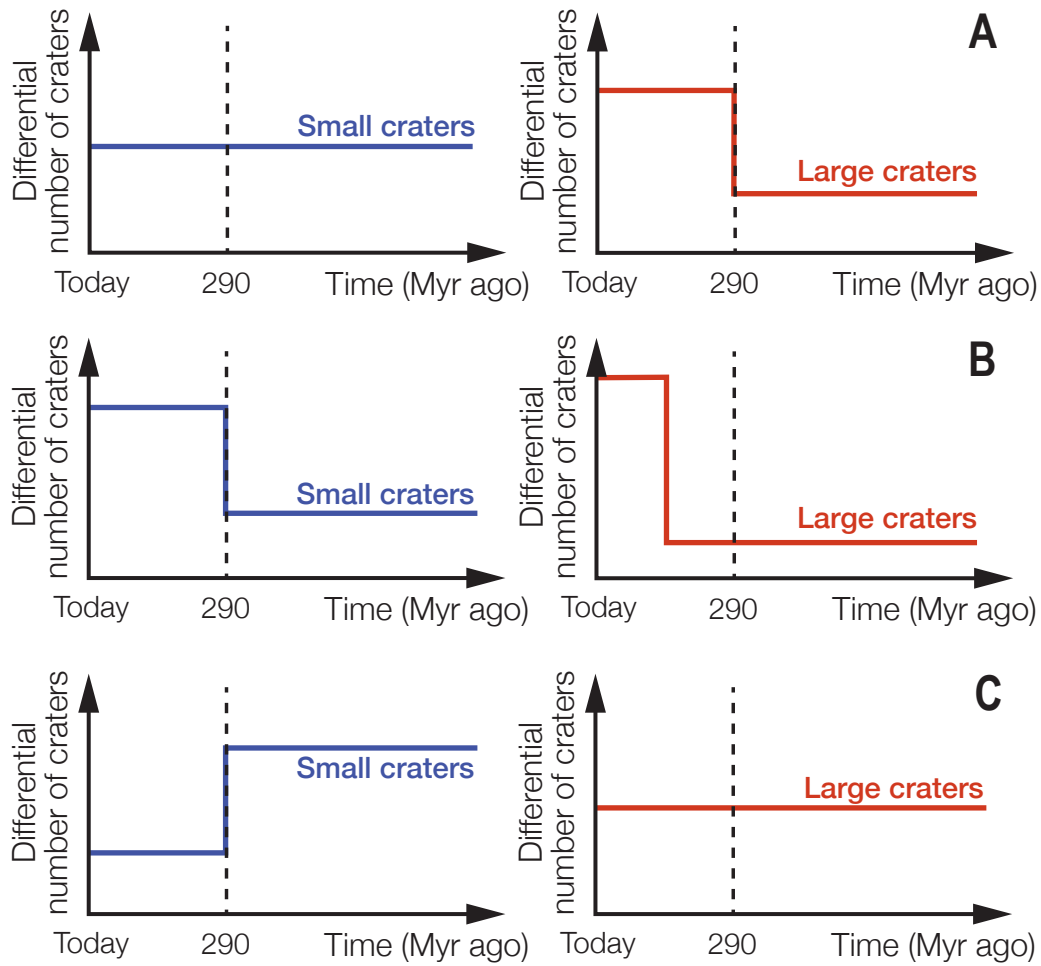


Fig. S2. Schematic illustration of different scenarios for the small and large crater production rate on the Moon. (A) Scenario A: Small and large crater production rates are decoupled, with the former constant and latter increasing at 290 Myr. **(B)** Scenario B: The small body and large crater production rates are coupled and constant. **(C)** Scenario C: The small and large crater production rates are decoupled, with the former decreasing 290 Myr and latter constant. Scenario A matches all available constraints and is therefore our adopted scenario.

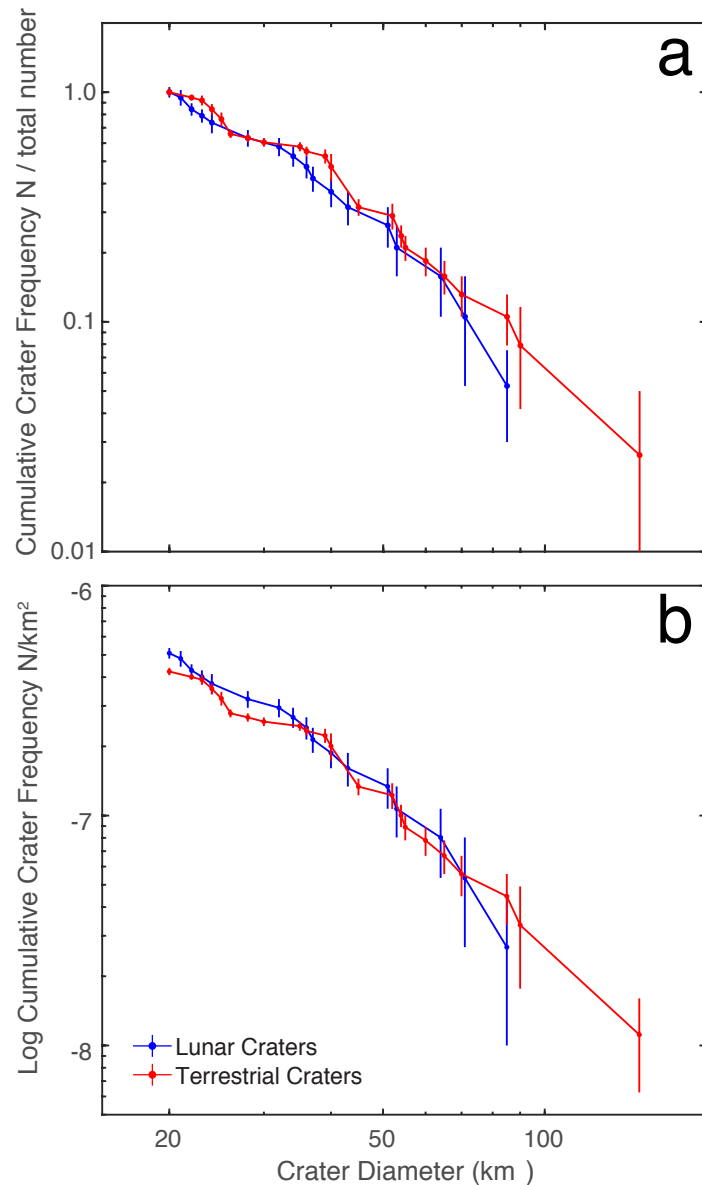


Fig. S3. Size frequency distribution of lunar and terrestrial craters. Cumulative size frequency distributions, normalized by number of craters, for lunar (blue symbols) and terrestrial (red symbols) craters (Tables S1 and S2) with diameter $D \geq 20$ km. **(A)** Populations normalized by total number. Error bars correspond to Poisson statistics of the cumulative numbers. **(B)** Populations normalized by sampled area (80°N to 80°S for the Moon, which represents 98.5% of the total surface area, and 11% of the Earth's total surface area, respectively) and adjusted for an Earth to Moon impact ratio of 1.6. In both plots, the two populations show very similar distributions, supporting the notion that the observed population of terrestrial craters does not show preservation bias as a function of size for $D \geq 20$ km craters.

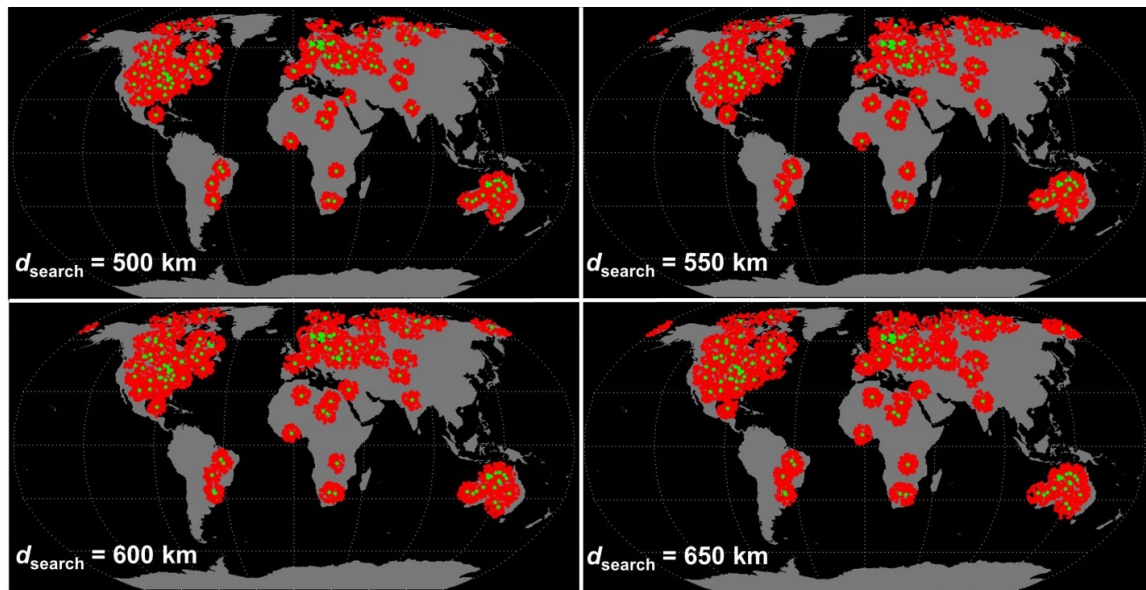


Fig. S4. Representative simulations of the crater counting area for the Earth. All terrestrial craters with $D \geq 5$ km are shown as green dots. The red dots represent random points on the globe (out of 30,000 points) than fall within $d_{\text{search}} = (500, 550, 600, 650$ km). The number of red dots divided by 30,000 yields the counting area of the Earth. The counting area was found to be 9.6%, 10.5%, 12.0%, 13.3%, respectively.

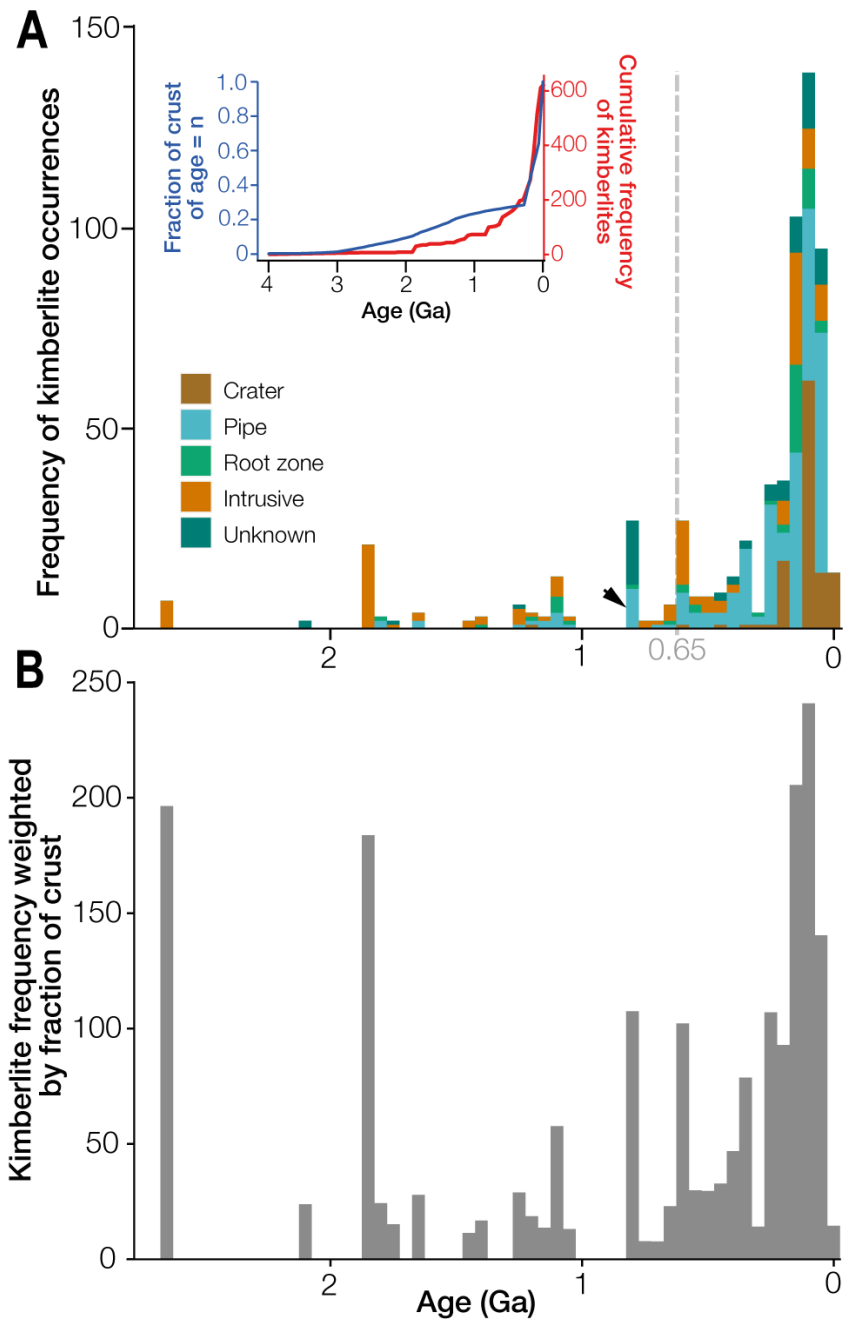


Fig. S5. Distribution of kimberlites through time. (A) Frequency distribution of kimberlites with well-constrained ages (i.e., with radiometric or stratigraphic control; $n = 624$). Arrow indicates kimberlite pipes that were buried soon after emplacement in the intra-cratonic Kimberley Basin, Western Australia. Inset: cumulative frequency distribution of kimberlite occurrences (red line); also shown is the fraction of the Earth's crust of a given age (blue line) (65), where the cumulative total (1.0) equals the total area of the crust, or $5.1 \times 10^8 \text{ km}^2$. **(B)** Distribution of kimberlites weighted by the fraction of Earth's crust of a particular age (see inset to A). A pronounced peak in the Mesozoic Era (c. 252 to 66 million years ago) is associated with intensified kimberlite magmatism accompanying breakup of the Pangaea supercontinent (66).

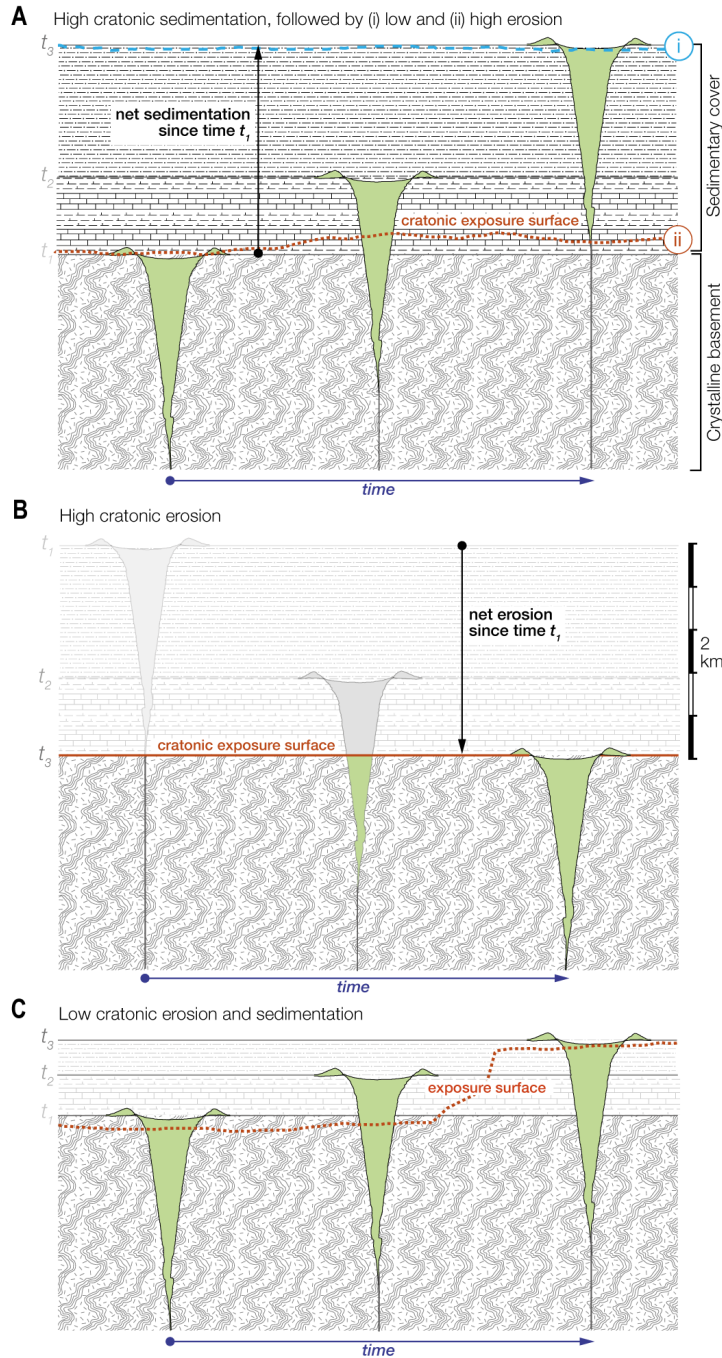


Fig. S6. Schematic diagrams showing the likely effect of background cratonic erosion and sedimentation on the kimberlite and impact crater records, at three hypothetical time intervals from t_1 to t_3 . (A) High cratonic sedimentation followed by negligible erosion (scenario *i*) leads to exposure of only the youngest kimberlite pipes and craters (shown in green). However, high erosion rates (scenario *ii*) leads to exposure of young intrusives and older craters and pipes. (B) High cratonic erosion produces a record dominated by old intrusives and only the youngest kimberlite pipes and craters. (C) Low cratonic erosion and sedimentation (*I2*) is necessary to explain the occurrence of kimberlite pipes of all ages since 650 Myr (Fig. S5).

Table S1.

List of rocky lunar craters with $D \geq 10$ km and their ages determined from the regression, updated from (2).

Names	Lon (°)	Lat (°)	D (km)	Age (Myr)
Copernicus (C)	340	10	97	797
Tycho (T)	349	-43	86	85
King (K)	120	5	76	992
Jackson (J)	197	22	71	147
Ohm	246	18	64	291
Anaxagoras	350	73	53	586
Crookes	195	-10	52	446
Glushko	282	8	43	196
Aristarchus (A)	313	24	40	164
Necho (N)	123	-5	37	80
Das	223	-27	36	657
Petavius B	57	-20	34	224
Thales	50	62	32	61
Kepler	322	8	32	930
Proclus	47	16	28	253
Lalande	351	-4	24	495
Moore F (MF)	185	37	24	41
Larmor Q	176	29	23	178

Giordano Bruno (GB)	103	36	22	4
Schwabe F	50	66	21	814
Innes G	122	27	21	527
Cleostratus J	276	61	21	443
No name	239	-68	21	272
No name	152	15	19	449
No name	117	-20	19	209
Dionysius	17	3	19	492
Byrgius A (BA)	296	-25	19	47
Sundman V	266	12	18	93
Dawes	26	17	18	454
Ventris M	158	-6	18	391
Epigenes A	360	67	18	347
No name	201	1	17	173
Carrel	27	11	17	295
No name	245	-22	16	221
Mandel'shtam F	166	5	16	44
Ryder	143	-44	16	140
Janssen K	42	-46	16	175
Gauss J	73	41	16	191

No name	206	48	15	138
No name	136	67	15	313
Rayet Y	113	47	15	40
Hume Z	90	-4	15	981
No name	141	75	15	31
Fechner T	123	-59	15	33
Geminus C	59	34	14	800
No name	80	23	14	993
No name	211	28	14	56
No name	192	12	14	290
No name	183	49	14	377
Nicolai A	24	-42	14	669
No name	263	44	14	1026
Tharp	146	-31	14	22
No name	143	1	13	318
No name	129	-67	13	26
Dugan J	108	61	13	159
Sirsalis F	300	-14	13	629
Darney C	334	-14	13	582
Aitken A	173	-14	13	259
Egede A	11	52	13	84

No name	251	15	13	113
Mosting A	355	-3	13	1324
Pythagoras K	284	67	13	732
O'Day M	157	-32	13	436
No name	215	6	13	678
No name	82	26	13	406
No name	166	36	12	645
Cauchy	39	10	12	489
Papaleksi Q	163	10	12	343
No name	210	-12	12	181
Pico B	345	47	12	612
Mohorovicic F	197	-19	12	385
No name	72	-63	12	539
No name	174	60	12	145
No name	227	-29	12	81
No name	200	-45	12	708
Lagrange D	287	-35	12	257
No name	190	10	12	407
Eichstadt G	279	-22	12	686
Gambart A	341	1	12	344
No name	162	-71	12	54

Furnerius A	59	-34	12	29
Beaumont D	26	-17	11	511
Goddard A	90	17	11	189
No name	177	16	11	39
Reimarus H	62	-49	11	640
No name	109	21	11	226
No name	254	-73	11	126
No name	218	-48	11	563
No name	73	-60	11	193
No name	236	44	11	369
Fraunhofer G	58	-39	11	454
No name	162	11	11	385
No name	35	23	11	873
Lagrange H	294	-29	11	583
Cameron	46	6	11	480
Alfraganus C	18	-6	11	433
Hilbert A	109	-16	11	301
No name	111	12	11	238
Avery	81	-1	11	139
Messier A	47	-2	11	128
Aratus	5	24	11	421

No name	94	-17	11	137
Euclides C	330	-13	11	50
No name	302	-70	11	13
Arnold G	31	67	10	223
Bessarion	323	15	10	164
No name	207	35	10	587
Democritus A	32	62	10	218
Mercurius H	63	49	10	181
No name	132	-37	10	110
No name	234	14	10	34

Table S2.

List of terrestrial craters with $D \geq 20$ km and younger than 650 Myr, updated from (24).

Names	D (km)	Age (Myr)(24)	Updated Age
Acraman	90	590	
Araguainha	40	255	
Beaverhead	60	600	
Boltysh	24	65	
Carswell	39	115	485 (66)
Charlevoix	54	450	
Chesapeake Bay	40	35	

Chicxulub	150	66	
Clearwater East	26	465	
Clearwater West	36	290	
Gosses Bluff	22	142	145 (67)
Haughton	23	23	
Kamensk	25	49	
Kara	65	70	
Kara-Kul	52	5	Likely < 50 (69) *
Lappaj_rvi	23	76	
Logancha	20	40	
Manicouagan	85	214	
Manson	35	74	
Mistastin	28	36	
MjÀlnir	40	142	
Montagnais	45	51	
Morokweng	70	145	
Obolon'	20	169	
Popigai	90	36	
Presqu'ile	24	500	
Pucezh-Katunki	40	167	193 (71)
Ries	24	15	

Rochechouart	23	201	
Saqqa	39	240	
Saint Martin	40	220	228 (72)
Siljan	52	376.8	390 (73)**
Slate Islands	30	450	
Steen River	25	91	
Strangways	25	646	
Tookoonoka	55	128	
Tunnunik (Prince Albert)	25	290	
Woodleigh	40	364	

* The age of Karakul crater is unknown, but it is younger than the India-Asia collision 55-60 Myr ago (70).

** The reported age for Siljan crater is ~380 Myr or ~400 Myr (73). Here, we used an average age of ~390 Myr.

References and Notes

1. J. L. Bandfield, R. R. Ghent, A. R. Vasavada, D. A. Paige, S. J. Lawrence, M. S. Robinson, Lunar surface rock abundance and regolith fines temperatures derived from LRO diviner radiometer data. *J. Geophys. Res. Planets* **116**, E00H02 (2011). [doi:10.1029/2011JE003866](https://doi.org/10.1029/2011JE003866)
2. R. R. Ghent, P. O. Hayne, J. L. Bandfield, B. A. Campbell, C. C. Allen, L. M. Carter, D. A. Paige, Constraints on the recent rate of lunar ejecta breakdown and implications for crater ages. *Geology* **42**, 1059–1062 (2014). [doi:10.1130/G35926.1](https://doi.org/10.1130/G35926.1)
3. Materials and methods are available as supplementary materials.
4. G. H. Heiken, D. T. Vaniman, B. M. French, *Lunar Sourcebook—A User's Guide to the Moon* (Cambridge Univ. Press, 1991).
5. R. J. Pike, Depth/diameter relations of fresh lunar craters—Revision from spacecraft data. *Geophys. Res. Lett.* **1**, 291–294 (1974). [doi:10.1029/GL001i007p00291](https://doi.org/10.1029/GL001i007p00291)
6. T. S. Culler, T. A. Becker, R. A. Muller, P. R. Renne, Lunar impact history from $^{40}\text{Ar}/^{39}\text{Ar}$ dating of glass spherules. *Science* **287**, 1785–1788 (2000). [doi:10.1126/science.287.5459.1785](https://doi.org/10.1126/science.287.5459.1785) [Medline](#)
7. N. Zellner, J. Delano, $^{40}\text{Ar}/^{39}\text{Ar}$ ages of lunar impact glasses: Relationships among Ar diffusivity, chemical composition, shape, and size. *Geochim. Cosmochim. Acta* **161**, 203–218 (2015). [doi:10.1016/j.gca.2015.04.013](https://doi.org/10.1016/j.gca.2015.04.013)
8. C. I. Fassett, B. J. Thomson, Crater degradation on the lunar maria: Topographic diffusion and the rate of erosion on the moon. *J. Geophys. Res. Planets* **119**, 2255–2271 (2014). [doi:10.1002/2014JE004698](https://doi.org/10.1002/2014JE004698)
9. A. S. McEwen, J. M. Moore, E. M. Shoemaker, The Phanerozoic impact cratering rate: Evidence from the farside of the Moon. *J. Geophys. Res. Planets* **102** (E4), 9231–9242 (1997). [doi:10.1029/97JE00114](https://doi.org/10.1029/97JE00114)
10. J. A. Grier, A. S. McEwen, P. G. Lucey, M. Milazzo, R. G. Strom, Optical maturity of ejecta from large rayed lunar craters. *J. Geophys. Res. Planets* **106** (E12), 32847–32862 (2001). [doi:10.1029/1999JE001160](https://doi.org/10.1029/1999JE001160)
11. R. A. F. Greive, E. M. Shoemaker, The record of past impacts on Earth, in *Hazards Due to Comets and Asteroids* (Univ. Arizona Press, 1995), pp 417–462.
12. T. J. Blackburn, S. A. Bowring, J. T. Perron, K. H. Mahan, F. O. Dudas, K. R. Barnhart, An exhumation history of continents over billion-year time scales. *Science* **335**, 73–76 (2012). [doi:10.1126/science.1213496](https://doi.org/10.1126/science.1213496) [Medline](#)
13. E. I. Smith, Determination of origin of small lunar and terrestrial craters by depth diameter ratio. *J. Geophys. Res.* **76**, 5683–5689 (1971). [doi:10.1029/JB076i023p05683](https://doi.org/10.1029/JB076i023p05683)
14. R. S. J. Sparks, L. Baker, R. J. Brown, M. Field, J. Schumacher, G. Stripp, A. Walters, Dynamical constraints on kimberlite volcanism. *J. Volcanol. Geotherm. Res.* **155**, 18–48 (2006). [doi:10.1016/j.jvolgeores.2006.02.010](https://doi.org/10.1016/j.jvolgeores.2006.02.010)
15. L. Wilson, J. W. Head III, An integrated model of kimberlite ascent and eruption. *Nature* **447**, 53–57 (2007). [doi:10.1038/nature05692](https://doi.org/10.1038/nature05692) [Medline](#)

16. R. J. Brown, G. A. Valentine, Physical characteristics of kimberlite and basaltic intraplate volcanism and implications of a biased kimberlite record. *Geol. Soc. Am. Bull.* **125**, 1224–1238 (2013). [doi:10.1130/B30749.1](https://doi.org/10.1130/B30749.1)
17. P. F. Hoffman, A. J. Kaufman, G. P. Halverson, D. P. Schrag, A neoproterozoic snowball earth. *Science* **281**, 1342–1346 (1998). [doi:10.1126/science.281.5381.1342](https://doi.org/10.1126/science.281.5381.1342) [Medline](#)
18. C. B. Keller *et al.*, Neoproterozoic glacial origin of the Great Unconformity. *Proc. Natl. Acad. Sci. U.S.A.* 10.1073/pnas.1804350116 (2019).
19. M. S. DeLucia, W. R. Guenther, S. Marshak, S. N. Thomson, A. K. Ault, Thermochronology links denudation of the Great Unconformity surface to the supercontinent cycle and snowball Earth. *Geology* **46**, 167–170 (2017). [doi:10.1130/G39525.1](https://doi.org/10.1130/G39525.1)
20. R. A. F. Grieve, W. U. Reimold, J. Morgan, U. Riller, M. Pilkington, Observations and interpretations at Vredefort, Sudbury, and Chicxulub: Towards an empirical model of terrestrial impact basin formation. *Meteorit. Planet. Sci.* **43**, 855–882 (2008). [doi:10.1111/j.1945-5100.2008.tb01086.x](https://doi.org/10.1111/j.1945-5100.2008.tb01086.x)
21. W. F. Bottke, D. Vokrouhlický, D. Nesvorný, An asteroid breakup 160 Myr ago as the probable source of the K/T impactor. *Nature* **449**, 48–53 (2007). [doi:10.1038/nature06070](https://doi.org/10.1038/nature06070) [Medline](#)
22. D. Vokrouhlický, W. F. Bottke, D. Nesvorný, Forming the flora family: Implications for the near-Earth asteroid population and large terrestrial planet impactors. *Astron. J.* **153**, 172 (2017). [doi:10.3847/1538-3881/aa64dc](https://doi.org/10.3847/1538-3881/aa64dc)
23. Paige *et al.*, LRO DLRE LEVEL 5 GDR V1.0, NASA Planetary Data System, LRO-L-DLRE-5-GDR-V1.0 (2011); <https://pds.nasa.gov/ds-view/pds/viewDataset.jsp?dsid=LRO-L-DLRE-5-GDR-V1.0>; retrieved 22 July 2016.
24. “Earth Impact Database,” Planetary and Space Science Centre (PASSC), University of New Brunswick; www.passc.net/EarthImpactDatabase; retrieved 22 July 2016.
25. S. Faure, CONSOREM Database (Version 3), Consortium de Recherche en Exploration Minérale CONSOREM, Université du Québec à Montréal; www.consorem.ca (2010); retrieved 22 July 2016.
26. M. Zanetti, A. Stadermann, B. Jolliff, H. Hiesinger, C. H. van der Bogert, J. Plescia, Evidence for self-secondary cratering of Copernican-age continuous ejecta deposits on the moon. *Icarus* **298**, 64–77 (2017). [doi:10.1016/j.icarus.2017.01.030](https://doi.org/10.1016/j.icarus.2017.01.030)
27. H. Sato, M. S. Robinson, B. Hapke, B. W. Denevi, A. K. Boyd, Resolved Hapke parameter maps of the Moon. *J. Geophys. Res. Planets* **119**, 1775–1805 (2014). [doi:10.1002/2013JE004580](https://doi.org/10.1002/2013JE004580)
28. United States Geological Survey, Geologic Province Map; <https://earthquake.usgs.gov/data/crust/type.html>; retrieved 5 March 2018.
29. Geological Survey of Canada, “Generalized geological map of the world and linked databases,” technical report 2915d (1995).

30. J. L. Bandfield, J. T. S. Cahill, L. M. Carter, C. D. Neish, G. W. Patterson, J.-P. Williams, D. A. Paige, Distal ejecta from lunar impacts: Extensive regions of rocky deposits. *Icarus* **283**, 282–299 (2017). [doi:10.1016/j.icarus.2016.05.013](https://doi.org/10.1016/j.icarus.2016.05.013)
31. D. Foreman-Mackey, D. W. Hogg, D. Lang, J. Goodman, emcee: The MCMC hammer. *Astron. Soc. Pacific* **125**, 306–312 (2013). [doi:10.1086/670067](https://doi.org/10.1086/670067)
32. J. K. Pritchard, M. T. Seielstad, A. Perez-Lezaun, M. W. Feldman, Population growth of human Y chromosomes: A study of Y chromosome microsatellites. *Mol. Biol. Evol.* **16**, 1791–1798 (1999). [doi:10.1093/oxfordjournals.molbev.a026091](https://doi.org/10.1093/oxfordjournals.molbev.a026091) [Medline](#)
33. J. M. Marin, P. Pudlo, C. P. Robert, R. J. Ryder, Approximate Bayesian computational methods. *Stat. Comput.* **22**, 1167–1180 (2012). [doi:10.1007/s11222-011-9288-2](https://doi.org/10.1007/s11222-011-9288-2)
34. A. H. Parker, The intrinsic Neptune Trojan orbit distribution: Implications for the primordial disk and planet migration. *Icarus* **247**, 112–125 (2015). [doi:10.1016/j.icarus.2014.09.043](https://doi.org/10.1016/j.icarus.2014.09.043)
35. H. Jeffreys, An invariant form for the prior probability in estimation problems. *Proc. R. Soc. London A Math. Phys. Sci.* **186**, 453–461 (1946). [doi:10.1098/rspa.1946.0056](https://doi.org/10.1098/rspa.1946.0056) [Medline](#)
36. F. W. Scholz, M. A. Stephens, K-Sample Anderson-Darling Tests. *J. Am. Stat. Assoc.* **82**, 918–924 (1987).
37. V. C. Sousa, M. Fritz, M. A. Beaumont, L. Chikhi, Approximate bayesian computation without summary statistics: The case of admixture. *Genetics* **181**, 1507–1519 (2009). [doi:10.1534/genetics.108.098129](https://doi.org/10.1534/genetics.108.098129) [Medline](#)
38. C. P. Robert, J. M. Cornuet, J. M. Marin, N. S. Pillai, Lack of confidence in approximate Bayesian computation model choice. *Proc. Natl. Acad. Sci. U.S.A.* **108**, 15112–15117 (2011). [doi:10.1073/pnas.1102900108](https://doi.org/10.1073/pnas.1102900108) [Medline](#)
39. H. Jeffries, *Theory of Probability* (Clarendon Press, 1961).
40. G. Neukum, B. A. Ivanov, W. K. Hartmann, Cratering records in the inner solar system in relation to the lunar reference system. *Space Sci. Rev.* **96**, 55–86 (2001). [doi:10.1023/A:1011989004263](https://doi.org/10.1023/A:1011989004263)
41. D. Stoffler *et al.*, Cratering history and lunar chronology. *Rev. Mineral. Geochem.* **60**, 519–596 (2006). [doi:10.2138/rmg.2006.60.05](https://doi.org/10.2138/rmg.2006.60.05)
42. H. Hiesinger, C. H. van der Bogert, J. H. Pasckert, L. Funcke, L. Giacomini, L. R. Ostrach, M. S. Robinson, How old are young lunar craters? *J. Geophys. Res. Planets* **117** (E12), E00H10 (2012). [doi:10.1029/2011JE003935](https://doi.org/10.1029/2011JE003935)
43. S. J. Robbins, New crater calibrations for the lunar crater-age chronology. *Earth Planet. Sci. Lett.* **403**, 188–198 (2014). [doi:10.1016/j.epsl.2014.06.038](https://doi.org/10.1016/j.epsl.2014.06.038)
44. J. P. Williams, C. H. van der Bogert, A. V. Pathare, G. G. Michael, M. R. Kirchoff, H. Hiesinger, Dating very young planetary surfaces from crater statistics: A review of issues and challenges. *Met. Planet. Sci.* **53**, 554–582 (2017). [doi:10.1111/maps.12924](https://doi.org/10.1111/maps.12924)
45. W. F. Bottke *et al.*, Debaised orbital and absolute magnitude distribution of the near-earth objects. *Icarus* **156**, 399–433 (2002). [doi:10.1006/icar.2001.6788](https://doi.org/10.1006/icar.2001.6788)

46. W. F. Bottke Jr., D. Vokrouhlicky, D. P. Rubincam, D. Nesvorny, The Yarkovsky and YORP Effects: Implications for asteroid dynamics. *Annu. Rev. Earth Planet. Sci.* **34**, 157–191 (2006). [doi:10.1146/annurev.earth.34.031405.125154](https://doi.org/10.1146/annurev.earth.34.031405.125154)
47. W. F. Bottke Jr., D. Durda, D. Nesvorny, R. Jedicke, A. Morbidelli, D. Vokrouhlicky, H. Levison, Linking the collisional history of the main asteroid belt to its dynamical excitation and depletion. *Icarus* **179**, 63–94 (2005). [doi:10.1016/j.icarus.2005.05.017](https://doi.org/10.1016/j.icarus.2005.05.017)
48. W. F. Bottke *et al.*, The collisional evolution of the asteroid belt, in *Asteroids IV*, P. Michel, F. DeMeo, W. F. Bottke, Eds. (Univ. Arizona Press, 2015), pp. 701–724.
49. M. Granvik, A. Morbidelli, R. Jedicke, B. Bolin, W. F. Bottke, E. Beshore, D. Vokrouhlický, M. Delbò, P. Michel, Super-catastrophic disruption of asteroids at small perihelion distances. *Nature* **530**, 303–306 (2016). [doi:10.1038/nature16934](https://doi.org/10.1038/nature16934) [Medline](#)
50. D. Nesvorný, D. Vokrouhlický, A. Morbidelli, W. F. Bottke, Asteroidal source of L chondrite meteorites. *Icarus* **200**, 698–701 (2009). [doi:10.1016/j.icarus.2008.12.016](https://doi.org/10.1016/j.icarus.2008.12.016)
51. J. R. Masiero, A. K. Mainzer, T. Grav, J. M. Bauer, R. Jedicke, Revising the age for the Baptistina asteroid family using WISE/NEOWISE data. *Astrophys. J.* **759**, 14 (2012). [doi:10.1088/0004-637X/759/1/14](https://doi.org/10.1088/0004-637X/759/1/14)
52. P. G. Brown, P. Wiegert, D. Clark, E. Tagliaferri, Orbital and physical characteristics of meter-scale impactors from airburst observations. *Icarus* **266**, 96–111 (2016). [doi:10.1016/j.icarus.2015.11.022](https://doi.org/10.1016/j.icarus.2015.11.022)
53. L. W. Bandermann, S. F. Singer, Calculation of meteoroid impacts on moon and earth. *Icarus* **19**, 108–113 (1973). [doi:10.1016/0019-1035\(73\)90142-5](https://doi.org/10.1016/0019-1035(73)90142-5)
54. D. W. Hughes, A new approach to the calculation of the cratering rate of the Earth over the last 125 ± 20 Myr. *Mon. Not. R. Astron. Soc.* **317**, 429–437 (2000). [doi:10.1046/j.1365-8711.2000.03568.x](https://doi.org/10.1046/j.1365-8711.2000.03568.x)
55. R. A. F. Grieve, E. M. Shoemaker, The record of past impacts on Earth, in *Hazards Due to Comets and Asteroids*, T. Gehrels, M. S. Matthews, A. M. Schumann, Eds. (Univ. Arizona Press, 1994).
56. E. M. Shoemaker, Impact cratering through geologic time. *J. R. Astron. Soc. Can.* **92**, 297–309 (1998).
57. D. E. Wilhelms, with sections by J. F. McCauley, N. J. Trask, “The geologic history of the moon,” technical report (USGS Professional Paper 1348, Denver, 1987).
58. B. R. Hawke, D. T. Blewett, P. G. Lucey, G. A. Smith, J. F. Bell III, B. A. Campbell, M. S. Robinson, The origin of lunar crater rays. *Icarus* **170**, 1–16 (2004). [doi:10.1016/j.icarus.2004.02.013](https://doi.org/10.1016/j.icarus.2004.02.013)
59. P. G. Lucey, D. T. Blewett, G. J. Taylor, B. R. Hawke, Imaging of lunar surface maturity. *J. Geophys. Res. Planets* **105** (E8), 20377–20386 (2000). [doi:10.1029/1999JE001110](https://doi.org/10.1029/1999JE001110)
60. J. K. Harmon, M. A. Slade, B. J. Butler, J. W. Head III, M. S. Rice, D. B. Campbell, Mercury: Radar images of the equatorial and midlatitude zones. *Icarus* **187**, 374–405 (2007). [doi:10.1016/j.icarus.2006.09.026](https://doi.org/10.1016/j.icarus.2006.09.026)

61. C. D. Neish, D. T. Blewett, J. K. Harmon, E. I. Coman, J. T. S. Cahill, C. M. Ernst, A comparison of rayed craters on the Moon and Mercury. *J. Geophys. Res. Planets* **118**, 2247–2261 (2013). [doi:10.1002/jgre.20166](https://doi.org/10.1002/jgre.20166)
62. R. H. Mitchell, *Kimberlites: Mineralogy, Geochemistry, and Petrology* (Plenum Press, 1986).
63. R. M. Flowers, B. Schoene, (U-Th)/He thermochronometry constraints on unroofing of the eastern Kaapvaal craton and significance for uplift of the southern African Plateau. *Geology* **38**, 827–830 (2010). [doi:10.1130/G30980.1](https://doi.org/10.1130/G30980.1)
64. J. Braun, F. Guillocheau, C. Robin, G. Baby, H. Jelsma, Rapid erosion of the Southern African Plateau as it climbs over a mantle superswell. *J. Geophys. Res. Solid Earth* **119**, 6093–6112 (2014). [doi:10.1002/2014JB010998](https://doi.org/10.1002/2014JB010998)
65. C. Johnson, T. J. Bowling, Where have all the craters gone? Earth's bombardment history and the expected terrestrial cratering record. *Geology* **42**, 587–590 (2014). [doi:10.1130/G35754.1](https://doi.org/10.1130/G35754.1)
66. T. H. Torsvik, K. Burke, B. Steinberger, S. J. Webb, L. D. Ashwal, Diamonds sampled by plumes from the core-mantle boundary. *Nature* **466**, 352–355 (2010). [doi:10.1038/nature09216](https://doi.org/10.1038/nature09216) [Medline](#)
67. C. Alwmark, W. Bleeker, A. LeCheminant, L. Page, A. Schersten, An Early Ordovician ^{40}Ar - ^{39}Ar age for the ~50 km Carswell impact structure, Canada. *Geol. Soc. Am.* **129**, 1442–1449 (2017).
68. D. J. Milton, J. F. Sutter, Revised age for the Gosses Bluff impact structure, Northern Territory, Australia, based on $^{40}\text{Ar}/^{39}\text{Ar}$ dating. *Meteoritics* **22**, 281–289 (1987). [doi:10.1111/j.1945-5100.1987.tb00625.x](https://doi.org/10.1111/j.1945-5100.1987.tb00625.x)
69. E. P. Gurov, E. P. Gurova, The Kurakul depression in the Pamirs—A reliable impact structure. *Geologicheskii Zhurnal* **6**, 53–64 (1993).
70. X. Hu, E. Garzanti, J. Wang, W. Huang, W. An, A. Webb, The timing of India-Asia collision onset – Facts, theories, controversies. *Earth Sci. Rev.* **160**, 264–299 (2016). [doi:10.1016/j.earscirev.2016.07.014](https://doi.org/10.1016/j.earscirev.2016.07.014)
71. M. M. Meier, S. Holm-Alwmark, A tale of clusters: No resolvable periodicity in the terrestrial impact cratering record. *Mon. Not. R. Astron. Soc.* **467**, 2545–2551 (2017).
72. M. Schmieder, F. Jourdan, E. Tohver, E. A. Cloutis, E.A., $^{40}\text{Ar}/^{39}\text{Ar}$ age of the Lake Saint Martin impact structure (Canada)—Unchaining the Late Triassic terrestrial impact craters. *Earth Planet. Sci. Lett.* **406**, 37–48 (2014). [doi:10.1016/j.epsl.2014.08.037](https://doi.org/10.1016/j.epsl.2014.08.037)
73. F. Jourdan, W. U. Reimold, Age of the Siljan impact structure. *Meteoritics and Planetary Science Supplement*, **75**, abstract no. 5093 (2012).